Nanoscale Advances

PAPER

View Article Online
View Journal | View Issue

Cite this: *Nanoscale Adv.*, 2020, **2**, 332

Effects of methylamine doping on the stability of triple cation $(FA_{0.95-x}MA_xCs_{0.05})PbI_3$ single crystal perovskites†

Yimin Huang,[ab] Li Zhao, *[ab] Jin Li,*[ab] Fang Lu[ab] and Shimin Wang[ab]

Received 28th October 2019
Accepted 13th November 2019

DOI: 10.1039/c9na00682f

rsc.li/nanoscale-advances

Despite being promising photovoltaic materials, widespread use of organic–inorganic halide perovskite materials is still hindered by their undesirable stability. To cope with this challenge, methylamine (MA) is doped into triple cation perovskite single crystals of $(FA_{0.95-x}MA_xCs_{0.05})PbI_3$, and cesium-containing triple cation perovskite single crystals with five different MA molar ratios (x = 0, 0.05, 0.10, 0.15, and 0.20) are synthesized and characterized. Among them, $(FA_{0.8}MA_{0.15}Cs_{0.05})PbI_3$ shows high stability against water-oxygen and light for 60 days, and the thermal decomposition temperature of $(FA_{0.8}MA_{0.15}Cs_{0.05})PbI_3$ reaches as high as 305 °C. Besides, the carrier lifetime of $(FA_{0.8}MA_{0.15}Cs_{0.05})PbI_3$ is up to 5.957 μs, which remains as 5.646 μs (95%) after 60 days of light illumination. This work studies the stability of perovskite single crystals based on $(FA_{0.95-x}MA_xCs_{0.05})PbI_3$ compositions and provides a reference for the discovery of novel perovskite photovoltaic devices with high efficiency and long-term stability.

Introduction

Perovskite solar cells (PSCs) have received wide attention due to their easy preparation[1–9] and ever-increasing photoelectric conversion efficiency (PCE).[10–14] Currently, the certified highest PCE of PSCs has reached 25.2%.[15] The high light absorption[16] and tunable cation components[17–19] of perovskites make them promising for application in PSCs. However, compared with commercial silicon-based solar cells (with more than 20 years of service life),[20] the undesirable stability of PSCs still hinders their rapid development and widespread use. The performance of perovskite photovoltaic devices was threatened by light, heat and water-oxygen,[21–25] and the main reason is the instability of the perovskite material itself. For example, $MAPbI_3$ perovskite was reported to be sensitive to moisture[26–28] and temperature.[29–31] $FAPbI_3$ (ref. 32 and 33) perovskite easily decomposes into yellow phase δ-$FAPbI_3$ at room temperature, which leads to the loss of optical properties. Snaith[34] reported that replacing some of the formamidinium (FA) in $FAPbI_3$ with methylamine (MA), forming (FA/MA)PbI_3 perovskite, can efficiently inhibit its phase separation and enhance the stability of the perovskite. Besides, doping an appropriate amount of cesium (Cs) ions can reduce trap state density and further improve the thermal stability of (FA/MA)PbI_3 perovskite. The introduction of the Cs ion can inhibit the formation of yellow phase $FAPbI_3$ due to its smaller radius. However, excessive doping of Cs will lead to the decrease of crystal size and induce phase decomposition forming $CsPbI_3$.[32,35–37] According to the literature reports, doping a trace amount of Cs ions would be optimal for (FA/MA)PbI_3 perovskite.

In addition, most of the studies on PSCs are based on polycrystalline films with pores, grain boundaries and defects,[38–42] resulting in severe hysteresis and environmental sensitivity,[43] which are detrimental to electron transport in perovskites and long-term stability[44] of PSCs. Nowadays, single crystal perovskites have drawn a lot of attention in the development of PSCs,[45] and perovskites with low defect states and suitable optical band gaps benefit both the photovoltaic performance and long-term stability of PSCs. Compared with polycrystalline thin films, $FAPbI_3$ single crystal perovskite has good thermal resistance,[46] but the optical properties and carrier drift of the $FAPbI_3$ single crystal material are seriously affected by its easy decomposition into yellow phase δ-$FAPbI_3$.[47] $MAPbI_3$ single crystal perovskite is the most widely used because of its excellent photoelectric performance, and the formation of (FA/MA)PbI_3 perovskite can effectively improve the structural stability.[48] And after doping a small amount of Cs ion into the $FAPbI_3$ single crystal perovskite, the density of defect states is reduced.[49] Thus, doping a trace amount of Cs ions into (FA/MA)PbI_3 single crystal perovskite would lead to better performance than the polycrystalline counterpart.

[a]Hubei Collaborative Innovation Center for Advanced Organic Chemical Materials, Wuhan 430062, PR China. E-mail: zhaoli7376@163.com; lijin238@126.com

[b]Ministry-of-Education Key Laboratory for the Green Preparation and Application of Functional Materials, Faculty of Materials Science and Engineering, Hubei University, Wuhan 430062, PR China

† Electronic supplementary information (ESI) available. See DOI: 10.1039/c9na00682f

In this work, a series of mixed cation perovskites $(FA_{0.95-x}MA_xCs_{0.05})PbI_3$ were prepared as single crystals, and a systematic study of their long-term stability, including water-oxygen, light and thermal stability was carried out, respectively. Related optimization effects were investigated and discussed in this paper. And the optimal cation doping ratio was determined based on the characterization of the properties of the materials. Cesium-containing triple cation perovskite single crystals with excellent stability and a long carrier lifetime were obtained, and they can be used as light absorption layers in high PCE and stable PSCs.

Experimental section

Materials

CH_3NH_3I (MAI, ≥ 99.5%), $NH_2CH{=}NH_2I$ (FAI, ≥99.5%) and PbI_2 (>99.99%) were purchased from Xi'an Polymer Light Technology Corp. CsI (99.999%) was purchased from Shanghai Mater Win New Materials Co., Ltd. The solvent of γ-butyrolactone (GBL, 99%) was purchased from Aladdin. All the materials were used as received.

Growth of perovskite single crystals

A series of $(FA_{0.95-x}MA_xCs_{0.05})PbI_3$ single crystals were prepared using the inverse temperature crystallization (ITC) method. $(FA_{0.95}Cs_{0.05})PbI_3$ and $(FA_{0.9}MA_{0.05}Cs_{0.05})PbI_3$ can be acquired from the 1.2 M clear GBL solution, and $(FA_{0.85}MA_{0.1}Cs_{0.05})PbI_3$, $(FA_{0.8}MA_{0.15}Cs_{0.05})PbI_3$ and $(FA_{0.75}MA_{0.2}Cs_{0.05})PbI_3$ can be acquired from the 1.6 M clear GBL solution. Crystal samples were gradually heated on a thermal stirrer (IKA C-MAG HS 7) to find the complete dissolution temperature and the crystallization temperature, and during this process the solution will change from a clear yellow solution to a black suspension, as shown in ESI Video 1.† The growth temperature of each crystal composition can be precisely and efficiently determined by this method. And the perovskite samples were slowly heated from the complete melting temperature to the crystallization temperature with 1 °C/30 min. Finally, the perovskite samples were sintered at the crystallization temperature for 3 hours, and all the parameters are listed in Table 1.

Perovskite single crystal alloy characterization

EDS mapping of the perovskite single crystal powders was performed using a field-emission scanning electron microscope (SEM) (Jeol JEM 6510LV). The X-ray diffraction (XRD) spectra were obtained using a Bruker-AXS D8 Advance X-ray diffractometer. Absorbance was tested using a UV-vis spectrophotometer (UV 3600, Shimadzu). Steady-state photoluminescence (PL) experiments were performed using an FLSP920 spectrometer (Edinburgh Instruments Ltd), and transient PL measurements were carried out using an FLS 980E fluorometer. The PL spectra were measured with a 485 nm laser as the excitation light source. Thermogravimetric Analysis (TGA) was carried out on a Mettler-TGA1 to characterize the thermal stability of the samples. And the long-term stability, water and oxygen stability, and light and thermal stability of the perovskite single crystal samples were evaluated, respectively. For the water and oxygen stability tests, the perovskite single crystal powders were put in a brown desiccator with a humidity of 20% and characterized intermittently for 60 days. For the light stability tests, the perovskite single crystal powders were stored in a self-made sealed box filled with argon, and kept in an ultraviolet aging box (Q-Lab, USA) for 60 days to conduct the "Day and Night" simulation test. After 12 hour illumination, the samples were kept in the dark for 12 hours, and the above-mentioned treatments were repeated. The device performances were measured under ambient conditions (15% < relative humidity (RH) < 60%) every time.

Results and discussion

Cs containing triple cation $(FA_{0.95-x}MA_xCs_{0.05})PbI_3$ perovskite single crystals were synthesized as shown in Fig. 1. EDS mapping was carried out on the single crystal powders (Fig. 2), and the uniform distribution of the Cs element indicates the successful doping of the Cs element into the $(FA_{0.8}MA_{0.15}Cs_{0.05})PbI_3$ perovskite. In order to analyze the crystal structure of the perovskites, the powder samples were subjected to XRD tests. As shown in Fig. 3a, diffraction peaks at 11.6° were detected from $(FA_{0.95}Cs_{0.05})PbI_3$, $(FA_{0.9}MA_{0.05}Cs_{0.05})PbI_3$ and $(FA_{0.85}MA_{0.1}Cs_{0.05})PbI_3$ samples, and can be assigned to the (010) plane of the yellow phase δ-$FAPbI_3$. And the 11.6° peak disappeared when the MA doping ratio reached 0.15, which suggests that yellow phase δ-$FAPbI_3$ formation can be efficiently inhibited with the addition of the MA cation (Fig. 3a). And the strong peaks at 14.1°, 28.3° and 31.8°, assigned to (110), (220) and (310) planes, proved the successful synthesis of cesium-containing triple cation perovskite single crystals. The magnified XRD pattern of the (110) plane is displayed in Fig. 3b. Obviously, all diffraction peaks demonstrate a shift to a high degree, and this is due to the smaller radius of the MA (2.17 Å) ions compared to the FA (2.53 Å) ions and the

Table 1 The growth parameters of perovskite single crystal systems

Samples	Solution concentration (mol L^{-1})	Temperature
$(FA_{0.95}Cs_{0.05})PbI_3$	1.2	70–120 °C
$(FA_{0.9}MA_{0.05}Cs_{0.05})PbI_3$	1.2	50–100 °C
$(FA_{0.85}MA_{0.1}Cs_{0.05})PbI_3$	1.6	75–125 °C
$(FA_{0.8}MA_{0.15}Cs_{0.05})PbI_3$	1.6	60–110 °C
$(FA_{0.75}MA_{0.2}Cs_{0.05})PbI_3$	1.6	70–120 °C

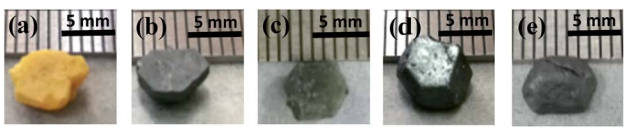

Fig. 1 Photographs of the series of $(FA_{0.95-x}MA_xCs_{0.05})PbI_3$ perovskite single crystals: (a) $(FA_{0.95}Cs_{0.05})PbI_3$, (b) $(FA_{0.9}MA_{0.05}Cs_{0.05})PbI_3$, (c) $(FA_{0.85}MA_{0.1}Cs_{0.05})PbI_3$, (d) $(FA_{0.8}MA_{0.15}Cs_{0.05})PbI_3$ and (e) $(FA_{0.75}MA_{0.2}Cs_{0.05})PbI_3$.

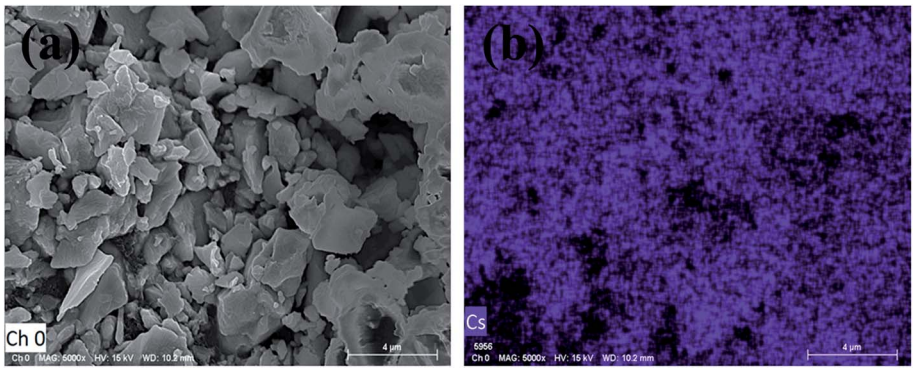

Fig. 2 (a) FESEM image of perovskite single crystals of $(FA_{0.8}MA_{0.15}Cs_{0.05})PbI_3$. (b) EDS mapping of the Cs element.

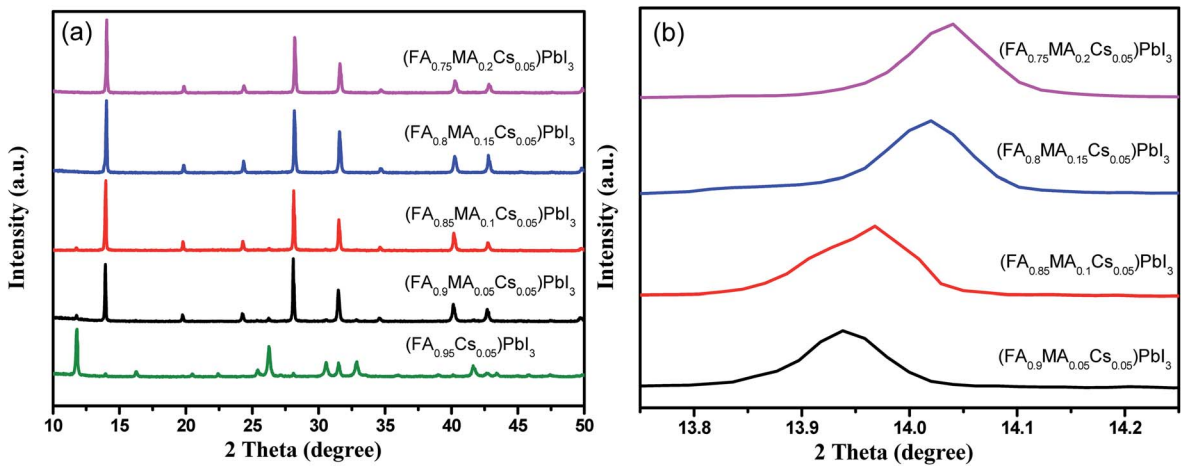

Fig. 3 XRD patterns of (a) $(FA_{0.95}Cs_{0.05})PbI_3$, $(FA_{0.9}MA_{0.05}Cs_{0.05})PbI_3$, $(FA_{0.85}MA_{0.1}Cs_{0.05})PbI_3$, $(FA_{0.8}MA_{0.15}Cs_{0.05})PbI_3$ and $(FA_{0.75}MA_{0.2}Cs_{0.05})PbI_3$, and (b) magnified angles on the (110) plane.

partial replacement of the FA ions with MA ions in the perovskite structure, causing lattice shrinking.[50]

Fig. 4 shows the UV-vis absorption spectra of the perovskite single crystals. A single crystal perovskite with high absorption at 830 nm is obtained. With MA ion doping, the absorption intensity of the perovskite single crystal is significantly increased, which could be the reason for the formation of a black α-phase perovskite (as shown in Fig. 3a) resulting in higher light absorption.[51] According to the absorption spectra, the band gaps of the perovskite single crystals of $(FA_{0.9}MA_{0.05}Cs_{0.05})PbI_3$, $(FA_{0.85}MA_{0.1}Cs_{0.05})PbI_3$, $(FA_{0.8}MA_{0.15}Cs_{0.05})PbI_3$ and $(FA_{0.75}MA_{0.2}Cs_{0.05})PbI_3$ are estimated to be 1.42 eV, 1.44 eV, 1.45 eV and 1.455 eV respectively (Fig. 5a–d). With the increase of the molar ratio of MA cations, the band gaps of the perovskite single crystals are slightly widened, which can be attributed to the smaller radius of the MA cation compared to that of the FA cation.[52] Doping a smaller quantity of MA into the perovskite crystal structure shrinks the crystal lattice, according to the Bragg equation, and the XRD peaks shift to the right, corresponding to Fig. 3b, and the bandgap is widened.[53,54]

Emission peaks of single crystals of $(FA_{0.9}MA_{0.05}Cs_{0.05})PbI_3$, $(FA_{0.85}MA_{0.1}Cs_{0.05})PbI_3$, $(FA_{0.8}MA_{0.15}Cs_{0.05})PbI_3$ and $(FA_{0.75}MA_{0.2}Cs_{0.05})PbI_3$ at 830 nm are presented in Fig. 6a. $(FA_{0.8}MA_{0.15}Cs_{0.05})PbI_3$ with a 15% molar ratio of MA exhibits the highest PL intensity, indicating the least occurrence of

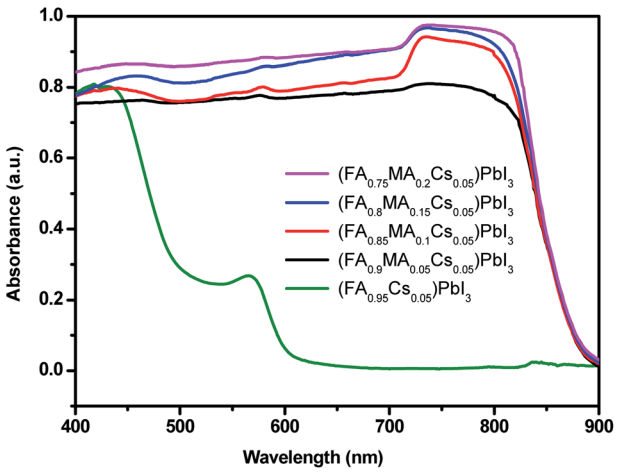

Fig. 4 UV-vis absorption spectra of $(FA_{0.95}Cs_{0.05})PbI_3$, $(FA_{0.9}MA_{0.05}Cs_{0.05})PbI_3$, $(FA_{0.85}MA_{0.1}Cs_{0.05})PbI_3$, $(FA_{0.8}MA_{0.15}Cs_{0.05})PbI_3$ and $(FA_{0.75}MA_{0.2}Cs_{0.05})PbI_3$.

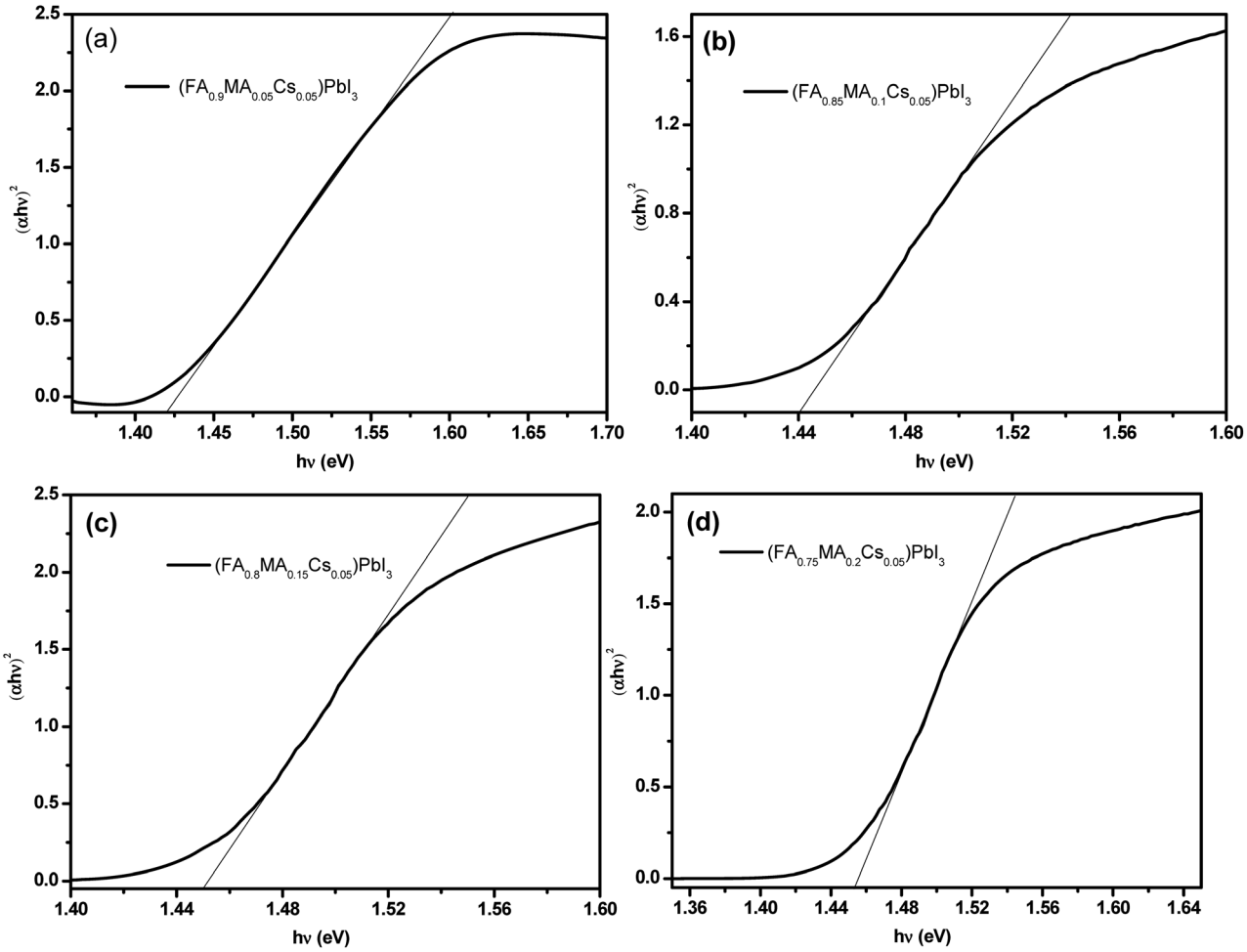

Fig. 5 Tauc plots of the five compositions of (a) $(FA_{0.9}MA_{0.05}Cs_{0.05})PbI_3$ (1.42 eV), (b) $(FA_{0.85}MA_{0.1}Cs_{0.05})PbI_3$ (1.44 eV), (c) $(FA_{0.8}MA_{0.15}Cs_{0.05})PbI_3$ (1.45 eV) and (d) $(FA_{0.75}MA_{0.2}Cs_{0.05})PbI_3$ (1.455 eV).

nonradiative recombination.[46] Moreover, transient PL measurements (Fig. 6b) are carried out to characterize the carrier lifetime of the perovskite crystals. All samples used for testing were fresh crystals. The average carrier lifetime of $(FA_{0.8}MA_{0.15}Cs_{0.05})PbI_3$ is as long as 5.957 μs, which is the highest among the average carrier lifetimes of the other three perovskite single crystal samples (5.030 μs of $(FA_{0.75}MA_{0.2}Cs_{0.05})PbI_3$, 4.120 μs of $(FA_{0.85}MA_{0.1}Cs_{0.05})PbI_3$ and 3.637 μs of

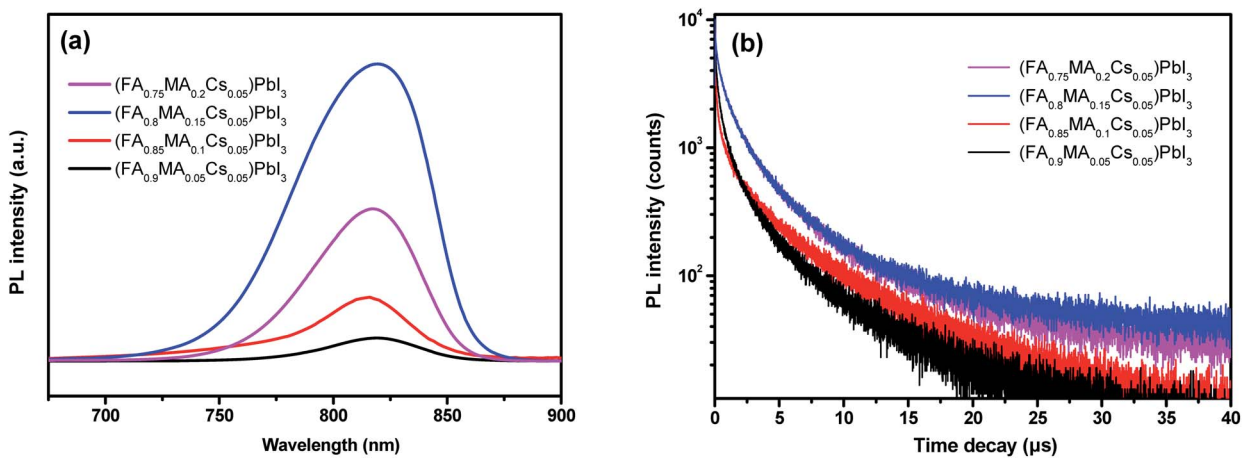

Fig. 6 The perovskite single crystals of $(FA_{0.9}MA_{0.05}Cs_{0.05})PbI_3$, $(FA_{0.85}MA_{0.1}Cs_{0.05})PbI_3$, $(FA_{0.8}MA_{0.15}Cs_{0.05})PbI_3$ and $(FA_{0.75}MA_{0.2}Cs_{0.05})PbI_3$ with (a) steady-state PL spectra and (b) transient photoluminescence spectra.

Table 2 The parameters of the time-resolved PL spectra of the perovskite single crystals: $(FA_{0.9}MA_{0.05}Cs_{0.05})PbI_3$, $(FA_{0.85}MA_{0.1}Cs_{0.05})PbI_3$, $(FA_{0.8}MA_{0.15}Cs_{0.05})PbI_3$ and $(FA_{0.75}MA_{0.2}Cs_{0.05})PbI_3$

Samples	τ_{ave} [μs]	τ_1 [μs]	τ_2 [μs]
$(FA_{0.9}MA_{0.05}Cs_{0.05})PbI_3$	3.637	5.336	1.259
$(FA_{0.85}MA_{0.1}Cs_{0.05})PbI_3$	4.120	6.092	1.523
$(FA_{0.8}MA_{0.15}Cs_{0.05})PbI_3$	5.957	8.234	1.808
$(FA_{0.75}MA_{0.2}Cs_{0.05})PbI_3$	5.030	7.098	1.617

$(FA_{0.9}MA_{0.05}Cs_{0.05})PbI_3$, and all parameters are summarized in Table 2).

In order to evaluate the water-oxygen stability of the perovskite single crystals, we placed the perovskite powders in a brown dryer and stored them in a dark environment, exposed to water (20% humidity) and oxygen. It is found that the $(FA_{0.9}MA_{0.05}Cs_{0.05})PbI_3$ sample gradually turns yellow, and $(FA_{0.85}MA_{0.1}Cs_{0.05})PbI_3$, $(FA_{0.8}MA_{0.15}Cs_{0.05})PbI_3$ and $(FA_{0.75}MA_{0.2}Cs_{0.05})PbI_3$ samples still remain black. After 60 days of water-oxygen treatment, phase characterization was carried out on all samples by XRD tests (Fig. 7). The peaks at 11.6° suggest δ-$FAPbI_3$ phase separation from $(FA_{0.9}MA_{0.05}Cs_{0.05})PbI_3$ and $(FA_{0.85}MA_{0.1}Cs_{0.05})PbI_3$ samples. By comparison, $(FA_{0.8}MA_{0.15}Cs_{0.05})PbI_3$ and $(FA_{0.75}MA_{0.2}Cs_{0.05})PbI_3$ samples still maintained their pure perovskite single crystal structure. With the incorporation of 15% and 20% MA (molar ratio), the long-term stability of the perovskite samples was efficiently enhanced. Doping a smaller quantity of MA into the perovskite crystal structure enables the promotion of the interaction between the cation and the inorganic octahedron, which reduces the defect state of perovskite crystals thus increasing the long-term water-oxygen stability of the crystals.[20]

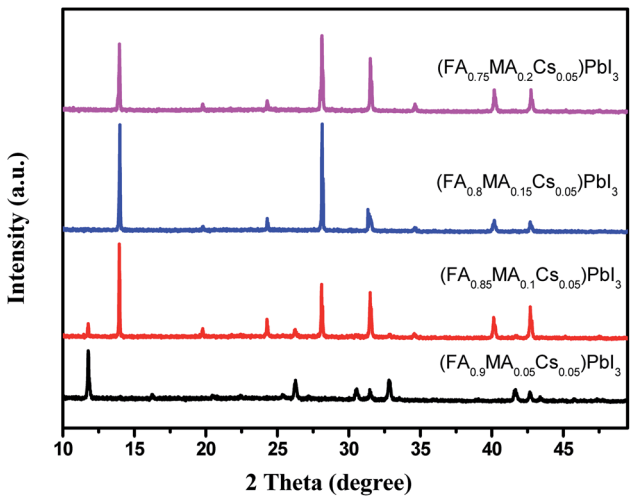

Fig. 7 XRD patterns of $(FA_{0.9}MA_{0.05}Cs_{0.05})PbI_3$, $(FA_{0.85}MA_{0.1}Cs_{0.05})PbI_3$, $(FA_{0.8}MA_{0.15}Cs_{0.05})PbI_3$ and $(FA_{0.75}MA_{0.2}Cs_{0.05})PbI_3$ after placing them for 60 days in contact with water-oxygen.

To investigate the long-term light stability of the perovskite crystals, the samples were placed in a self-made sealed transparent box filled with argon gas and under simulated illumination of day and night. After 60 days of "Day and Night" simulation test, the XRD characterization (Fig. 8a) reveals that $(FA_{0.9}MA_{0.05}Cs_{0.05})PbI_3$ and $(FA_{0.85}MA_{0.1}Cs_{0.05})PbI_3$ samples undergo phase decomposition while $(FA_{0.8}MA_{0.15}Cs_{0.05})PbI_3$ and $(FA_{0.75}MA_{0.2}Cs_{0.05})PbI_3$ show excellent light stability. The transient PL spectra of the pre-treated and post-treated $(FA_{0.8}MA_{0.15}Cs_{0.05})PbI_3$ perovskites are presented in Fig. 8b. After 60 days of light illumination, the post-treated $(FA_{0.8}MA_{0.15}Cs_{0.05})PbI_3$ sample still maintains a long carrier lifetime of 5.646 μs, which is 95% of the carrier lifetime of the pre-treated $(FA_{0.8}MA_{0.15}Cs_{0.05})PbI_3$ sample (5.957 μs). The above results show that the illumination causes only a small amount of defects in the $(FA_{0.8}MA_{0.15}Cs_{0.05})PbI_3$ perovskite crystal without phase separation.

The thermal stability of the perovskite crystals was investigated by TGA measurements. After the TGA test on $(FA_{0.8}MA_{0.15}Cs_{0.05})PbI_3$ (fresh crystal), two compositions of perovskite single crystals, namely $(MA_{0.95}Cs_{0.05})PbI_3$ and

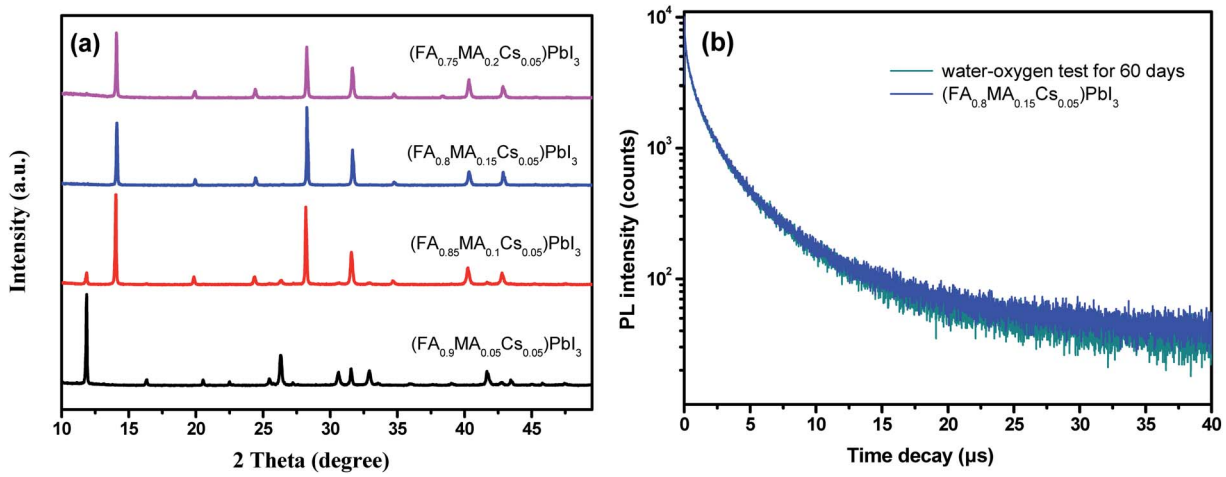

Fig. 8 (a) XRD patterns of $(FA_{0.9}MA_{0.05}Cs_{0.05})PbI_3$, $(FA_{0.85}MA_{0.1}Cs_{0.05})PbI_3$, $(FA_{0.8}MA_{0.15}Cs_{0.05})PbI_3$ and $(FA_{0.75}MA_{0.2}Cs_{0.05})PbI_3$ after illumination for 60 days. (b) Transient photoluminescence spectra of $(FA_{0.8}MA_{0.15}Cs_{0.05})PbI_3$ and the crystal under illumination for 60 days.

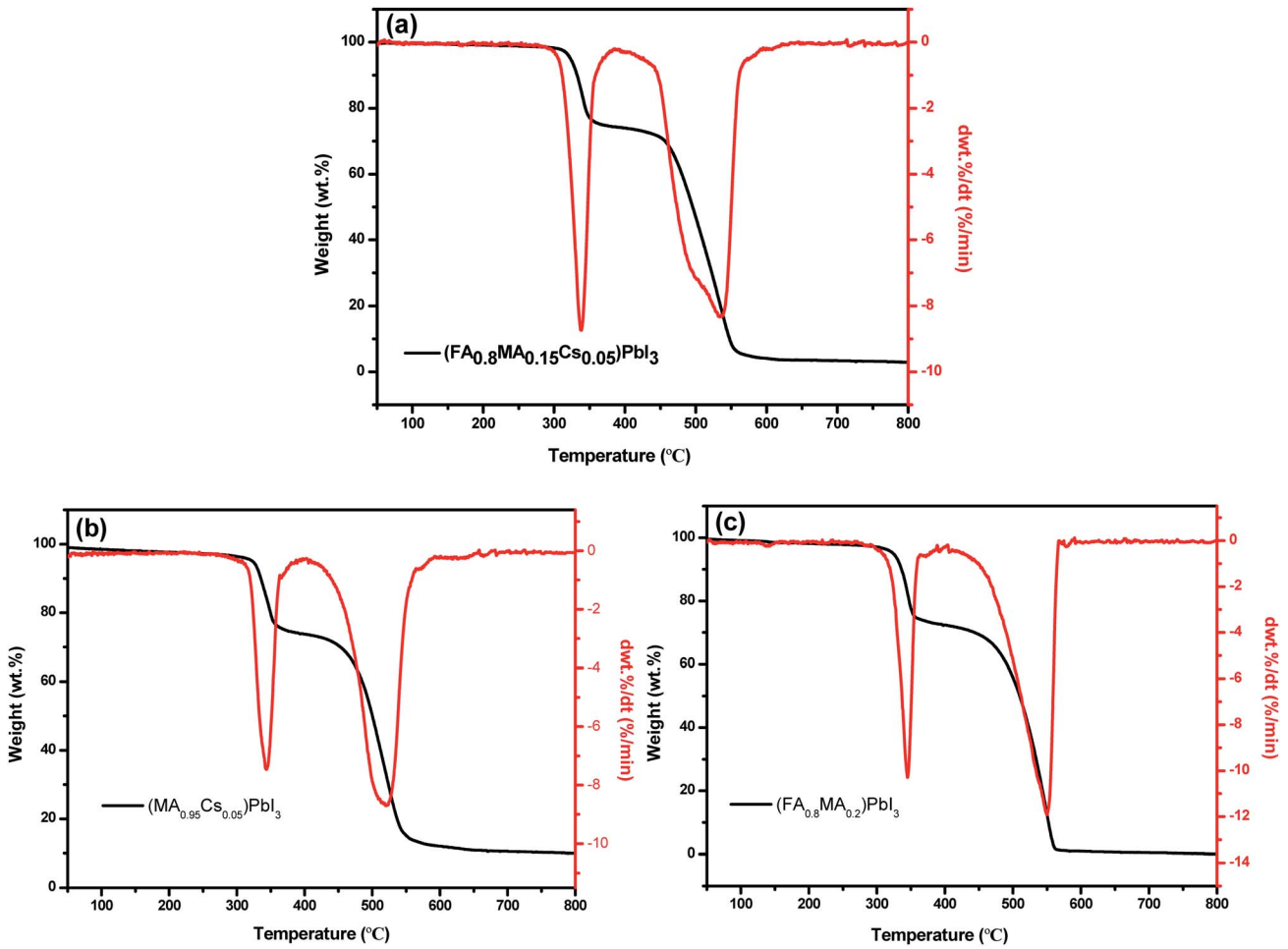

Fig. 9 TGA and DTA curves of perovskite single crystals: (a) $(FA_{0.8}MA_{0.15}Cs_{0.05})PbI_3$, (b) $(MA_{0.95}Cs_{0.05})PbI_3$ and (c) $(FA_{0.8}MA_{0.2})PbI_3$.

$(FA_{0.8}MA_{0.2})PbI_3$, were synthesized to investigate the effect of FA and Cs cation doping on the thermal stability of the perovskite. The TGA spectrum of $(FA_{0.8}MA_{0.15}Cs_{0.05})PbI_3$ is shown in Fig. 9a; the thermal decomposition temperature is 305 °C, which is close to that of pure $FAPbI_3$, and the weight loss of 20% between 305 and 360 °C can be attributed to the removal of organic components.[46,55,56] Lead halide is evaporated above 470 °C. By comparison, the removal of the organic component from $MAPbI_3$ occurs at 150–200 °C.[57–59] And the initial decomposition temperatures (Fig. 9b and c) of $(MA_{0.95}Cs_{0.05})PbI_3$ and $(FA_{0.8}MA_{0.2})PbI_3$ are 290 °C and 300 °C, respectively. Compared to the perovskite crystals of $(MA_{0.95}Cs_{0.05})PbI_3$ and $(FA_{0.8}MA_{0.2})PbI_3$, the better thermal stability of $(FA_{0.8}MA_{0.15}Cs_{0.05})PbI_3$ can be explained by the strong interaction between the cation and the inorganic octahedron. The initial decomposition temperature of the crystal without the FA cation decreased by 15 °C and the initial decomposition temperature without the Cs cation decreased by only 5 °C, which indicate that the FA cation has a stronger influence on the thermal stability of the crystal than the Cs cation, and this provides a reference for the synthesis of novel perovskite composition with excellent thermal stability.

Conclusions

In summary, we prepared a series of compositions of perovskite single crystals. Among them, $(FA_{0.8}MA_{0.15}Cs_{0.05})PbI_3$ perovskite maintains long-term stability after 60 days of water-oxygen and light treatment. The MA ion doping enabled a strong interaction between the cation and the inorganic octahedron, which efficiently improved the structural stability of the perovskite samples. The band gap of $(FA_{0.8}MA_{0.15}Cs_{0.05})PbI_3$ is 1.45 eV, which is very close to the optimal optical absorption band gap (1.1–1.4 eV); the carrier lifetime of $(FA_{0.8}MA_{0.15}Cs_{0.05})PbI_3$ perovskite single crystals reaches 5.957 μs, and the lifetime is still 5.646 μs after 60 days of light illumination. The thermal decomposition temperature of $(FA_{0.8}MA_{0.15}Cs_{0.05})PbI_3$ is as high as 305 °C. This study has provided a reference for the synthesis of perovskite single crystal materials with improved long-term stability and carrier lifetime, which are promising to be applied in high-efficiency and stable perovskite solar cells.

Conflicts of interest

There are no conflicts to declare.

Acknowledgements

This research was financially supported by the National Natural Science Foundation of China (51572072 and 5170021087) and the China Postdoctoral Science Foundation (2017M622384).

References

1 M. M. Lee, T. JoëL, M. Tsutomu, T. N. Murakami and H. J. Snaith, *Science*, 2012, **338**, 643–647.
2 J. Burschka, N. Pellet, S. J. Moon, R. Humphry-Baker, P. Gao, M. K. Nazeeruddin and M. Grätzel, *Nature*, 2013, **499**, 316.
3 L. Mingzhen, M. B. Johnston and H. Snaith, *Nature*, 2013, **501**, 395.
4 J. Nam Joong, N. Jun Hong, K. Young Chan, Y. Woon Seok, R. Seungchan and S. Sang, *Nat. Mater.*, 2014, **13**, 897–903.
5 N. J. Jeon, J. H. Noh, W. S. Yang, Y. C. Kim, S. Ryu, J. Seo and S. Seok, *Nature*, 2015, **517**, 476.
6 Y. Woon Seok, N. Jun Hong, J. Nam Joong, K. Young Chan, R. Seungchan, S. Jangwon and S. Seok, *Science*, 2015, **348**, 1234.
7 D. Bi, C. Yi, J. Luo, J. D. Décoppet, Z. Fei, S. M. Zakeeruddin, L. Xiong, A. Hagfeldt and M. Grätzel, *Nat. Energy*, 2016, **1**, 16142.
8 W. S. Yang, B.-W. Park, E. H. Jung, N. J. Jeon, Y. C. Kim, U. L. Dong, S. S. Shin, J. Seo, E. K. Kim and J. H. Noh, *Science*, 2017, **356**, 1376–1379.
9 D. Luo, W. Yang, Z. Wang, A. Sadhanala, Q. Hu, R. Su, R. Shivanna, G. F. Trindade, J. F. Watts and Z. Xu, *Science*, 2018, **360**, 1442–1446.
10 A. Mei, X. Li, L. Liu, Z. Ku, T. Liu, Y. Rong, M. Xu, M. Hu, J. Chen and Y. Yang, *Science*, 2014, **345**, 295–298.
11 H. Chen, F. Ye, W. Tang, J. He, M. Yin, Y. Wang, F. Xie, E. Bi, X. Yang and M. Grätzel, *Nature*, 2017, **550**, 92.
12 H. Tan, A. Jain, O. Voznyy, X. Lan, G. D. A. Fp, J. Z. Fan, R. Quintero-Bermudez, M. Yuan, B. Zhang and Y. Zhao, *Science*, 2017, **355**, 722–726.
13 Y. Rong, Y. Hu, A. Mei, H. Tan, M. I. Saidaminov, S. I. Seok, M. D. McGehee, E. H. Sargent and H. Han, *Science*, 2018, **361**, 8235.
14 S. Lin, H. Wang, X. Zhang, D. Wang, D. Zu, J. Song, Z. Liu, Y. Huang, K. Huang and N. Tao, *Nano Energy*, 2019, **62**, 111–116.
15 https://www.nrel.gov/pv/device-performance.html.
16 M. A. Green, A. Ho-Baillie and H. J. Snaith, *Nat. Photonics*, 2014, **8**, 506–514.
17 F. Hao, C. C. Stoumpos, D. H. Cao, R. P. H. Chang and M. G. Kanatzidis, *Nat. Photonics*, 2017, **8**, 489–494.
18 J. Kim, H. P. Kim, M. A. M. Teridi, A. R. B. M. Yusoff and J. Jin, *Sci. Rep.*, 2016, **6**, 37378.
19 X. Wang, Y. Cui, T. Li, M. Lei, J. Li and Z. Wei, *Adv. Opt. Mater.*, 2019, **7**, 1801274.
20 L. Chen, Y. Y. Tan, Z. X. Chen, T. Wang, S. Hu, Z. A. Nan, L.-Q. Xie, Y. Hui, J.-X. Huang and C. Zhan, *J. Am. Chem. Soc.*, 2019, **141**, 1665–1671.
21 Z. Gan, F. Zheng, W. Mao, C. Zhou, W. Chen, U. Bach, P. Tapping, T. W. Kee, J. A. Davis and B. Jia, *Nanoscale*, 2019, **11**, 14676–14683.
22 Q. Guo, F. Yuan, B. Zhang, S. Zhou, J. Zhang, Y. Bai, L. Fan, T. Hayat, A. Alsaedi and Z. a. Tan, *Nanoscale*, 2019, **11**, 115–124.
23 Y. Li, L. Zhao, M. Xiao, Y. Huang, B. Dong, Z. Xu, L. Wan, W. Li and S. Wang, *Nanoscale*, 2018, **10**, 22003–22011.
24 E. S. Parrott, J. B. Patel, A.-A. Haghighirad, H. J. Snaith, M. B. Johnston and L. M. Herz, *Nanoscale*, 2019, **11**, 14276–14284.
25 M. Xiao, L. Zhao, M. Geng, Y. Li, B. Dong, Z. Xu, L. Wan, W. Li and S. Wang, *Nanoscale*, 2018, **10**, 12141–12148.
26 J. Yang, B. D. Siempelkamp, D. Liu and T. L. Kelly, *ACS Nano*, 2015, **9**, 1955–1963.
27 Y. Rong, L. Liu, A. Mei, X. Li and H. Han, *Adv. Energy Mater.*, 2015, **5**, 1501066.
28 Y. Liu, S. Akin, L. Pan, R. Uchida, N. Arora, J. V. Milić, A. Hinderhofer, F. Schreiber, A. R. Uhl and S. M. Zakeeruddin, *Sci. Adv.*, 2019, **5**, 2543.
29 B. Conings, J. Drijkoningen, N. Gauquelin, A. Babayigit, J. D'Haen, L. D'Olieslaeger, A. Ethirajan, J. Verbeeck, J. Manca and E. Mosconi, *Adv. Energy Mater.*, 2015, **5**, 1500477.
30 G. Divitini, S. Cacovich, F. Matteocci, L. Cinà, A. D. Carlo and C. Ducati, *Nat. Energy*, 2016, 15012.
31 H. Wang, R. Liu, Y. Li, X. Lü, Q. Wang, S. Zhao, K. Yuan, Z. Cui, X. Li and S. Xin, *Joule*, 2018, **2**, 337–348.
32 Y. Yu, C. Wang, C. R. Grice, N. Shrestha, J. Chen, D. Zhao, W. Liao, A. J. Cimaroli, P. J. Roland and R. J. Ellingson, *Chemsuschem*, 2016, **9**, 3288.
33 P. Gratia, G. Grancini, J.-N. Audinot, X. Jeanbourquin, E. Mosconi, I. Zimmermann, D. Dowsett, Y. Lee, M. Grätzel and F. De Angelis, *J. Am. Chem. Soc.*, 2016, **138**, 15821–15824.
34 D. P. Mcmeekin, G. Sadoughi, W. Rehman, G. E. Eperon, M. Saliba, M. T. Hörantner, A. Haghighirad, N. Sakai, L. Korte, B. Rech, M. B. Johnston, L. M. Herz and H. J. Snaith, *Science*, 2016, **351**, 151.
35 M. Saliba, T. Matsui, J. Y. Seo, K. Domanski, J. P. Correa-Baena, M. K. Nazeeruddin, S. M. Zakeeruddin, W. Tress, A. Abate and A. Hagfeldt, *Energy Environ. Sci.*, 2016, **9**, 1989–1997.
36 L. T. Schelhas, Z. Li, J. A. Christians, A. Goyal and J. J. Berry, *Energy Environ. Sci.*, 2019, **12**, 1341–1348.
37 D. Kubicki, D. Prochowicz, A. Hofstetter, S. M. Zakeeruddin, M. Grätzel and L. Emsley, *J. Am. Chem. Soc.*, 2017, **139**, 7b07223.
38 Y. Huang, L. Zhao, Y. Li, W. Li and S. Wang, *Appl. Surf. Sci.*, 2019, **493**, 975–981.
39 D. Yang, Z. Yang, W. Qin, Y. Zhang, S. F. Liu and C. Li, *J. Mater. Chem. A*, 2015, **3**, 9401–9405.
40 E. L. Unger, E. T. Hoke, C. D. Bailie, W. H. Nguyen, A. R. Bowring, T. Heumüller, M. G. Christoforo and M. D. McGehee, *Energy Environ. Sci.*, 2014, **7**, 3690–3698.
41 F. Zheng, X. Hai, Y. Wang, Z. Zhao, Z. Lin, H. C. Cheng, S. J. Lee, G. Wang, Z. Feng and W. A. G. Iii, *Joule*, 2017, 117300302.
42 J. You, M. Lei, T. B. Song, T. F. Guo, Y. Yang, W. H. Chang, Z. Hong, H. Chen, H. Zhou and C. Qi, *Nat. Nanotechnol.*, 2015, **11**, 75–81.

43 Y. Zhang, Z. Zhou, F. Ji, Z. Li, G. Cui, P. Gao, E. Oveisi, M. K. Nazeeruddin and S. Pang, *Adv. Mater.*, 2018, **30**, 1707143.
44 M. I. Saidaminov, A. L. Abdelhady, B. Murali, E. Alarousu, V. M. Burlakov, W. Peng, I. Dursun, L. Wang, Y. He and G. Maculan, *Nat. Commun.*, 2015, **6**, 7586.
45 C. Wu, H. Li, Y. Yan, C. Bo, P. Jian, L. Jian, M. Sanghadasa and S. Priya, *Nano Energy*, 2017, **36**, 295–302.
46 Q. Han, S. H. Bae, P. Sun, Y. T. Hsieh, Y. Yang, Y. S. Rim, H. Zhao, Q. Chen, W. Shi and G. Li, *Adv. Mater.*, 2016, **28**, 2253–2258.
47 Z. Li, M. Yang, J.-S. Park, S.-H. Wei, J. J. Berry and K. Zhu, *Chem. Mater.*, 2015, **28**, 284–292.
48 C. Liu, K. Wang, C. Yi, X. Shi, A. W. Smith, X. Gong and A. J. Heeger, *Adv. Funct. Mater.*, 2016, **26**, 101–110.
49 H. Wang, H. Wu, Y. Xian, G. Niu, W. Yuan, H. Li, H. Yin, P. Liu, Y. Long and W. Li, *ACS Appl. Mater. Interfaces*, 2019, **11**, 13812–13821.
50 M. Saliba, T. Matsui, K. Domanski, J. Y. Seo, A. Ummadisingu, S. M. Zakeeruddin, J. P. Correa-Baena, W. R. Tress, A. Abate and A. Hagfeldt, *Science*, 2016, **354**, 206.
51 D. Prochowicz, R. Runjhun, M. M. Tavakoli, P. Yadav, M. Saski, A. Q. Alanazi, D. J. Kubicki, Z. Kaszkur, S. M. Zakeeruddin and J. Lewiński, *Chem. Mater.*, 2019, **31**, 1620–1627.
52 K. Wang, W. S. Subhani, Y. Wang, X. Zuo, H. Wang, L. Duan and S. Liu, *Adv. Mater.*, 2019, 1902037.
53 J. P. Correa-Baena, Y. Luo, T. M. Brenner, J. Snaider, S. Sun, X. Li, M. A. Jensen, L. Nienhaus, S. Wieghold and J. R. Poindexter, *Science*, 2019, **363**, 627–631.
54 M. S. D. Holanda, R. Szostak, P. E. Marchezi, L. G. T. A. Duarte and A. F. Nogueira, *Sol. RRL*, 2019, 1900199.
55 Y. Liu, Z. Yang, D. Cui, X. Ren, J. Sun, X. Liu, J. Zhang, Q. Wei, H. Fan and F. Yu, *Adv. Mater.*, 2015, **27**, 5176–5183.
56 O. Nazarenko, S. Yakunin, V. Morad, I. Cherniukh and M. V. Kovalenko, *NPG Asia Mater.*, 2017, **9**, 373.
57 E. J. Juarez-Perez, Z. Hawash, S. R. Raga, L. K. Ono and Y. Qi, *Energy Environ. Sci.*, 2016, **9**, 1039.
58 I. Deretzis, A. Alberti, G. Pellegrino, E. Smecca, F. Giannazzo, N. Sakai, T. Miyasaka and A. La Magna, *Appl. Phys. Lett.*, 2015, **106**, 131904.
59 B. Conings, J. Drijkoningen, N. Gauquelin, A. Babayigit, J. D'Haen, L. D'Olieslaeger, A. Ethirajan, J. Verbeeck, J. Manca and E. Mosconi, *Adv. Energy Mater.*, 2015, **5**, 1500477.